CONTRIBUTIONS to SCIENCE, **2** (2): 173-181 (2002)
Institut d'Estudis Catalans, Barcelona

Nanomechanics: A new approach for studying the mechanical properties of materials

F. Sanz*[1], J. Fraxedas[2], P. Gorostiza[1] and S. Garcia-Manyes[1]

1. Departament de Química Física i CBEN. Universitat de Barcelona
2. Institut de Ciència de Materials de Barcelona (CSIC), Bellaterra

Abstract

Atomic force spectroscopy was used to study the nanomechanical response to nanoindentations on the most stable face (100) of FCC brittle materials such as MgO and alkali halides. The layered expulsion of material demonstrates that brittle failure results from the critical stress brought on by plastic deformation and that plastic deformation consists of a series of discrete events. Due to the absence of indentation-induced dislocations, Young's modulus *E* can be correctly estimated from the elastic deformation region using simple mechanics. A new model is developed taking into account lateral interactions. Critical shear stress is also evaluated and discussed. As a result of the layered expulsion we also studied the nanomechanical response of surfaces of highly-oriented molecular organic thin films (ca. 1 μm thickness) because these are Van der Waals layered materials. The surfaces were again found to deform plastically and there were discrete discontinuities in the indentation curves, representing the molecular layers being expelled by the penetrating tip. Here, the Hertz model is quite good at revealing the role of lateral interactions in the indentation process. For the quasi-one-dimensional metal tetrathiafulvalene tetracyanoquinodimethane (TTF-TCNQ) the value of Young's modulus, $E \sim 20$ GPa, coincides with that obtained by other bulk methods. For the α-phase of the *p*-nitrophenyl nitronyl nitroxide (*p*-NPNN) radical, no information is available for single crystals and the estimated value obtained for the film is $E \sim 2$ GPa.

Resum

Mitjançant l'espectroscòpia de forces atòmiques s'ha estudiat la resposta nanomecànica a la nanoindentació de la superfície més estable d'un material trencadís FCC, com és ara el MgO (100). L'expulsió del material en forma de capes demostra que la fallida trencadissa implica, de fet, l'inici de la deformació plàstica o estrès crític, i que la deformació plàstica posterior consisteix en una sèrie d'esdeveniments discrets. Es pot determinar amb precisió el mòdul de Young, *E*, a partir de la regió de deformació elàstica mitjançant una mecànica senzilla, atesa l'absència de dislocacions induïdes per la nanoindentació. Amb aquesta finalitat s'ha desenvolupat un nou model fisicomatemàtic, que té en compte les interaccions laterals. El valor de l'estrès crític de fricció també s'ha calculat i comentat. Com a conseqüència d'aquesta expulsió en capes, també s'ha estudiat la resposta nanomecànica de superfícies de capes primes (gruix ~ 1 μm) de molècules orgàniques altament orientades, ja que es tracta de materials en capes amb interaccions de tipus Van der Waals. També en aquests materials la superfície es deforma plàsticament i presenta discontinuïtats discretes en les corbes d'indentació, associades ara a les capes moleculars expulsades per l'indentador. En el cas del metall quasiunidimensional tetratiofulvalè tetracianoquinodimetà (TTF-TCNQ), el valor del mòdul de Young, $E \sim 20$ GPa, coincideix amb l'obtingut per altres mètodes. En el cas de la fase α del radical *p*-nitrofenil nitronil nitròxid (*p*-NPNN) no es disposa d'informació per a monocristalls, i el valor obtingut per a les capes primes és de $E \sim 2$ GPa.

Keywords: Nanomechanics, brittle materials, molecular organic thin films, atomic force spectroscopy, mechanical properties

* Author for correspondence: Fausto Sanz, Departament de Química Física i CBEN, Universitat de Barcelona. Martí i Franquès 1. 08028 Barcelona, Catalonia (Spain). Tel. 34 934021240. Fax: 34 934021231. Email: sanz@qf.ub.es. Website: www.qf.ub.es/nano.

The mechanical properties of solids are illustrated classically by the behaviour of a uniform cross-section rod subjected to a uniaxial tension. A plot of the applied stress, $\sigma = F/S$, where *F* is the exerted force or load and *S* the cross-section area, against the linear strain ε, (fractional increase in length) gives the classical deformation curve (Fig. 1). This

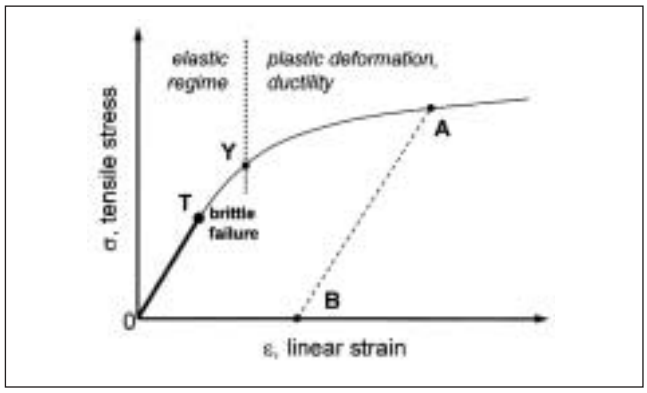

Figure 1. Usual tensile stress-strain curve, showing elastic deformation along OY, plastic yielding at Y and work hardening along YA. Brittle solids fail at a tensile stress T.

curve begins with an elastic deformation regime (OY line) where strains are small and Hooke's law is expected to apply: $\sigma = E\varepsilon$, E being Young's modulus. Above a given critical stress, σ_y, permanent plastic deformation occurs. If, at point A, we reduce the stress the material returns elastically to B. The strain OB gives the permanent plastic extension of the sample produced during the experiment. Full scale tensile tests to determine the strength properties of materials, as described in Fig. 1, are not easily done. Tensile specimens must be prepared and the experiment must be carried out at temperatures close to the melting point in order to measure significant strains [1].

Material engineers have, for decades, used a more convenient method of determining strength properties, namely, measuring the indentation hardness. A very hard indenter (i.e. a diamond pyramid in the Vickers test) will exert a plastic deformation (known as indentation) on the material surface under the action of a load F. The indented area, usually taken as the projected area, defines the mean pressure over the surface $p = F/S$. Experiments have clearly demonstrated that almost two-thirds of p plays no role in producing plastic flow, only one third of p produces the indentation. As a first approximation the applied pressure must be three times the uniaxial stress, for the given material, needed to produce permanent deformation, $p = 3\sigma_y$. The first hardness measurements used loads of a few kgs and produced indentation diameters of a few millimeters, so material hardness was expressed in kgf mm^{-2} and a hardness scale was established, with values ranging from 40 for polycrystalline copper, through 900 for ball-bearing steel, 2000 for sapphire and to over 10000 for diamond, all of them at room temperature.

More recently, indentation hardness has been used as a research tool with solids in order to identify the various constituents of an alloy or to estimate the amount of deformation produced by a particular metalworking process, including the creep properties. For such purposes the indentations must be small enough to resolve the examined features, what are known as microhardness measurements [2,3]. Typical loads lie between 0.1 and 10 N and indentation diameters of the test prove to be around 10-100 μm, easily and accurately measured by optical microscopy. An alternative approach is to measure the penetration depth of the indenter using highly accurate microdisplacement transducers [4]. From the geometry of the indenter the area can be calculated as a function of load, although corrections have to be made for elastic yielding and other topographical changes around the indentation. This approach has been useful for studying the properties of thin surface layers of metals deposited on hard surfaces, or the effect of ion implantation on semiconductors where the layer of interest may be less than 1 μm thick. Typical loads here are between 10^{-5} and 10^{-2} N. An important observation in microhardness measurements is that for metals the hardness tends to increase as the size of the indentation is reduced [5], and this is attributed to the limited range of dislocation movement available when very small volumes are involved. Plastic flow caused by indentation is associated with a critical shear stress connected to the material slice at an angle θ to the direction of the applied force F. This shear stress is then a fraction of the applied stress σ, $\tau = \sigma \cos\theta \sin\theta$, having a maximum value at $\theta = 45^{\circ}$ ($\tau = 0.5\ \sigma$). This is supported by the observation that plastic deformation is accompanied by atomic planes slipping over one another. Based on a constant value of the shear modulus G (defined as the ratio of the shear stress along the plane gliding over a contiguous plane and the shear strain), the maximum shear stress the lattice can withstand for a fcc single crystal would be only a small fraction of G (1/10 to 1/30). Consequently, with this observation, practically the whole of the work of plastic deformation dissipates as vibrational energy in the lattice, i. e. heat. Not more than a few per cent of the energy can be considered as retained strain energy in the lattice.

The indentation of metals is largely due to adhesion, shearing and deformation within and around the regions of real contact; in fact, it is a process that is often dominated by plastic flow around the contact zones. Thus, the smaller the indentation is, the more control over local features can be achieved; that is to say, a local area with control of surface defects can be chosen before indentation and the surface defects created by the indentation itself can be observed. Recently, valuable information about the mechanical properties of materials at the nanometer scale has been obtained [6,7]. Most of these studies have been focused on a ductile material, Au [8–10]. The indentation depths studied were mostly over 20 nm and a dislocation mechanism was argued to be responsible for the observed discrete events in indentation curves.

FCC brittle materials

The complete tensile behaviour shown in Fig. 1, where the specimen suffers continuous plastic deformation over the critical stress value σ_y, defines the material as ductile. Certain materials show no ductility. If we subject such materials to the tensile test, they stretch elastically and then snap at a certain critical stress value, causing what is known as brittle

failure. In an ideal homogeneous material, the brittle crack will be along a plane normal to the direction of the applied stress and σ_T would be the stress necessary to pull one plane of atoms completely away from a neighbouring plane. Brittle solids may be made ductile by applying a suitable hydrostatic pressure because the critical shear stress may be exceeded before the tensile stress is large enough to produce brittle failure. In this vein, it is interesting to note that in indentation hardness experiments a large hydrostatic component of the stress field is present and what appear to be plastic indentations have been reported, even though some cracking may also occur. The question is therefore whether it is really this large hydrostatic component of the stress field which inhibits brittle failure. Unlike with ductile materials, little work has been done on the nanometer-scale properties of ionic crystal surfaces [11-12]. We have previously studied the MgO(100) surface which, owing to its high stability, is increasingly used as a substrate for high-temperature superconductor thin films [13]. In spite of its technological relevance, however, only a few studies have dealt with the morphology and surface mobility of this surface [14, 15]. Indeed, with the exception of NaCl(100) [12(a)] there is little research on the surface relaxation processes of ionic crystals in general. The experiments that have been carried out show that relative humidity (RH) has a fundamental role with respect to the dynamic properties of ionic crystal surfaces exposed to normal atmospheric conditions [12(b)].

In this context, we have studied the nanomechanical properties and indentation mechanisms of MgO(100) for depths of only a few atomic layers. We found [16, 17] that plastic deformation of the crystal is indicated by discrete steps in the indentation curve and that these events are correlated with the number of atomic layers in the crystal which are expelled by the tip. Nanoindentations were performed in a controlled humidity chamber at 0 % measured RH and at room temperature. Under such conditions, adhesion forces and RH-related relaxation effects are practically avoided and Hertzian theory can be used *a priori* to analyse elastic properties [18,19]. A Nanoscope III atomic-force microscope (AFM) from Digital Instruments and Si microfabricated cantilevers from Nanosensors, having spring constants of 36 N m^{-1} and a nominal tip radius of less than 10 nm, were used for indenting and imaging. Nanoindentations were produced by extending and retracting the piezo while obtaining a force curve. For a given tip, results were reproducible on several locations of the sample. For different tips, results were comparable to the extent of uncertainty in the tip radius. It is known that friction effects, manifested as a hysteresis in the force curve, are also involved [20]. However, for such a hysteresis the unloading curve lies above the loading curve for a fixed position of the piezo, and therefore it can be discerned from our data. Errors due to piezohysteresis and non-linearity are minimized for small piezo displacements. Imaging was performed in the tapping mode™, both before and around 45s after the indentation. The low load tapping mode has the advantage of reducing friction between the tip and sample, and therefore reduces the possibility of displacing material expelled during the indentation. In order to check if noticeable tip deformation occurs as a result of the indentation process, the measured width of nearby MgO steps was compared before and after the indentation. No significant change was observed. Prior to indentation experiments, force curves on the surface of a diamond thin film were performed in order to take account of the maximum tip deformation during indentations. The slope of these force curves in the contact region was set to 1 and the slope of the brittle material force curves was then compared with it. Forces were estimated by multiplying the nominal elastic constant of the cantilever (36 Nm^{-1}) by the cantilever deflection. The penetration depth, δ, in the indentation curves was obtained by subtracting the cantilever deflection from the displacement of the piezo in the force curves [21].

Figure 2 shows an approach curve (cantilever deflection, Δ, vs. piezoscanner displacement, *z*) performed on a freshly cleaved NaCl (100) single crystal surface. No adherence is observed as the tip approaches the surface, indicating there is no detectable effect of adsorption phenomena. At a given point in the curve, plastic deformation is manifested by discrete events, which are associated with atomic layers being expelled by the tip penetrating the surface [17]. The effect of plasticity is evident in the inset of Fig. 2, which shows an AFM image taken after indentation with the same tip. A cavity surrounded by the expelled material can be seen.

Figure 3(a) shows the force curve and the corresponding derivative of a 5.5 nm-deep indentation, as shown by the profile in Fig. 3(b). Several discontinuities, identified by peaks in the force plot derivative, are observable in the force curves. The discontinuities produce a hysteresis in the force plot, and the unloading curve lies below the loading curve for a fixed position of the piezo. Following the arguments mentioned above, these discontinuities would correspond to atomic planes being expelled by the AFM tip during the indentation. The debris observed in the AFM image is thought to consist of nanocrystallites expelled during the nanoindentation [23]. The creation of dislocations was not observed on

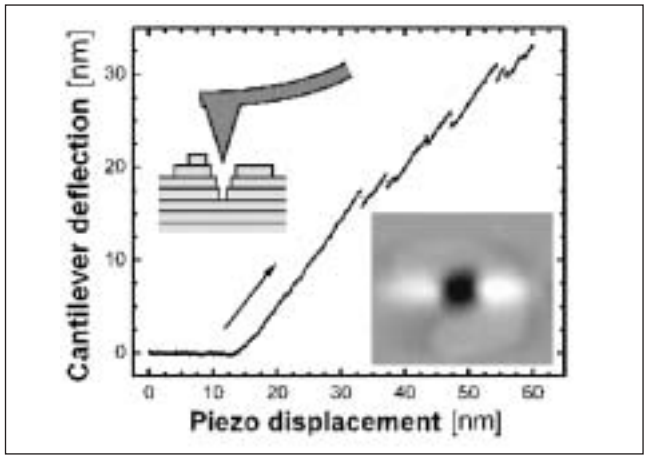

Figure 2. Cantilever deflection vs. piezo displacement curve for a freshly cleaved NaCl (100) single crystal surface. The upper inset shows a scheme of the indentation process. The lower inset shows a TMAFM image of the atomic layers expelled by the penetrating tip and the cavity which is generated.

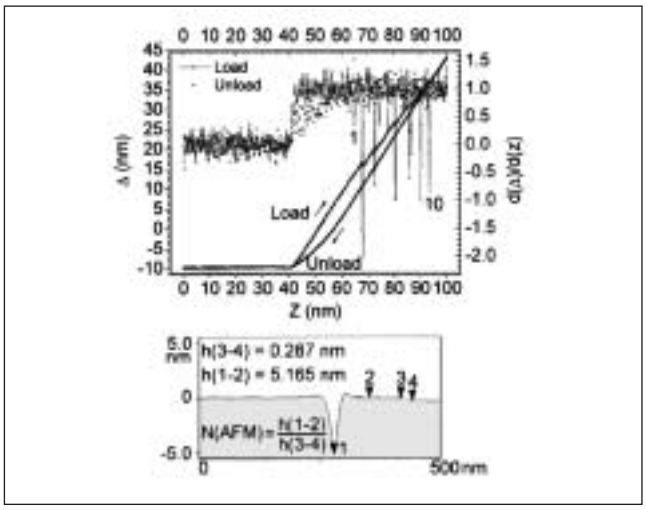

Figure 3. Force curve (deflection vs. piezo displacement) and its derivative for a monoatomic deep indentation. Arrows indicate the discontinuity in the force curve and the corresponding peak in its derivative. Inset: AFM image corresponding to the generated cavity. Cross section gives the depth of the cavity as compared with the monoatomic step height.

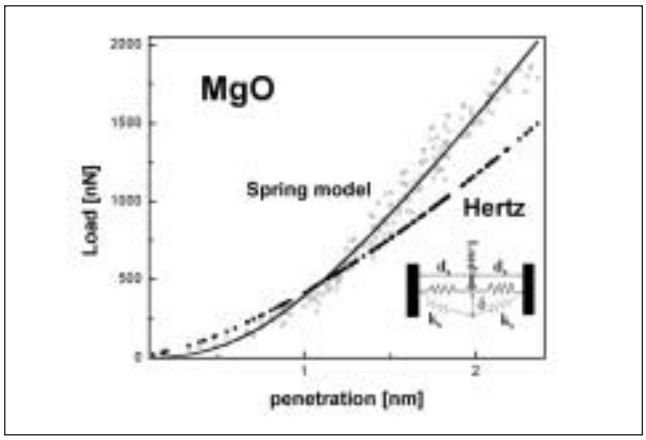

Figure 4. Nanoindentation curve for a MgO (100) single crystal surface [□]. Lines simulate the elastic region in terms of different models. (a) Hertz model, Eq. (1) in text, R = 7.5 nm, E^* = 113.2 GPa, (c) least-square fit to the proposed spring model (Eq. (2) in text). Inset gives the scheme of the proposed model with indication of the variables used.

the surface of the monocrystal during our experiments [24]. Note that in this case the distance between points 3 and 4 in Fig. 3(b), 0.287 nm, corresponding to the step's height, is exactly half of the lattice parameter, thus providing further evidence that it is indeed monoatomic steps which are being observed here.

Figure 4 corresponds to a nanoindentation curve (applied force or load vs. penetration) calculated from force plots like that of Fig. 2. Elastic responses to nanoindentations are usually analysed in terms of the Hertz model [25], which attempts to describe the deformation of the material through a flat area of contact. When the penetration is negligible compared with the indenter radius R ($\delta << R$), the applied force F for a paraboloid as a function of δ can be estimated by the expression [18, 19]:

$$F = 4/3\ E^*\ R^{1/2}\ \delta^{3/2}, \qquad (1)$$

where E^* stands for the reduced Young' s modulus defined as $1 / E^* = (1 - \nu_{tip}^2) / E_{tip} + (1 - \nu^2) / E$. The Poisson's ratios of the tip and surface are represented by ν_{tip} and ν, respectively, and Young' s moduli of the tip and surface by E_{tip} and E, respectively. In the case of MgO, E = 297 GPa and ν = 0.18 [26], and taking E_{tip} = 130 GPa and ν_{tip} = 0.28 for a silicon cantilever [27], we obtain E^* = 113.2 GPa. Taking the radius of the tip as 7.5 nm (< 10 nm as provided by the manufacturer) we simulated the Hertz curve in Fig. 4 using the value E^* = 113.2 GPa. This curve far from reproduces the experimental data points.

The failure of the Hertz model may be attributed to the fact that R is in the order of δ, a situation beyond the boundary conditions of the model. When $\delta << R$, it has been shown that the Hertz approximation seems to work quite well [28]. However, as described in the next section, experiments we carried out on layered molecular organic materials [29] found that the Hertz model fits the experimental data well. Since the main difference is that interaction strength is rather weak in all directions (Van der Waals interactions) for these organic materials, it seems reasonable to assume that the surface exhibits negligible deformation away from the tip during indentation. This is no longer true for ionic materials, where strong lateral coulombic forces play a key role.

In order to reproduce the experimental data we propose a model that takes into account the lateral forces in the deformed surface plane. The simplest way to model the dynamics of surface deformation is to consider the lateral interactions represented by two coupled aligned springs, constrained at both sides (see inset in Fig. 2), the spring constants k_s and length d_s at zero elongation being identical. The force applied at the contact mid-point perpendicularly to the alignment, as a function of the deformation δ, has been calculated to be $F(\delta) = 2k_s\ \delta\ (1 - d_s / \sqrt{(\delta^2 + d_s^2)})$. A general expression for surface isotropic systems is:

$$F(\delta) = k\ \delta\ (1 - d / \sqrt{(\delta^2 + d^2)}), \qquad (2)$$

where k and d stand for an equivalent spring constant and a coherence length, respectively. The mathematical deduction of the spring model is shown in Figure 5. The experimental fit to this model for a freshly cleaved MgO (100) surface is shown in Fig. 4, while Fig. 6 shows the same for KCl (100) surfaces. The model reproduces the experimental points quite well. For the alkali halide single crystals the nanoindentation experiments were also performed in Ar flow for freshly cleaved surfaces, but with lower spring constant cantilevers (k_c ~ 14 Nm^{-1}, from NT-MDT, Russia). The elastic regions of NaCl, KCl and KBr monocrystal curves were obtained with these cantilevers because they enable higher sensitivity than the stiffer ones (~36 Nm^{-1}) used for MgO, and vice-versa. The nanoindentation curve for a freshly cleaved KCl(100) surface shown in Figure 6 clearly illustrates what has been

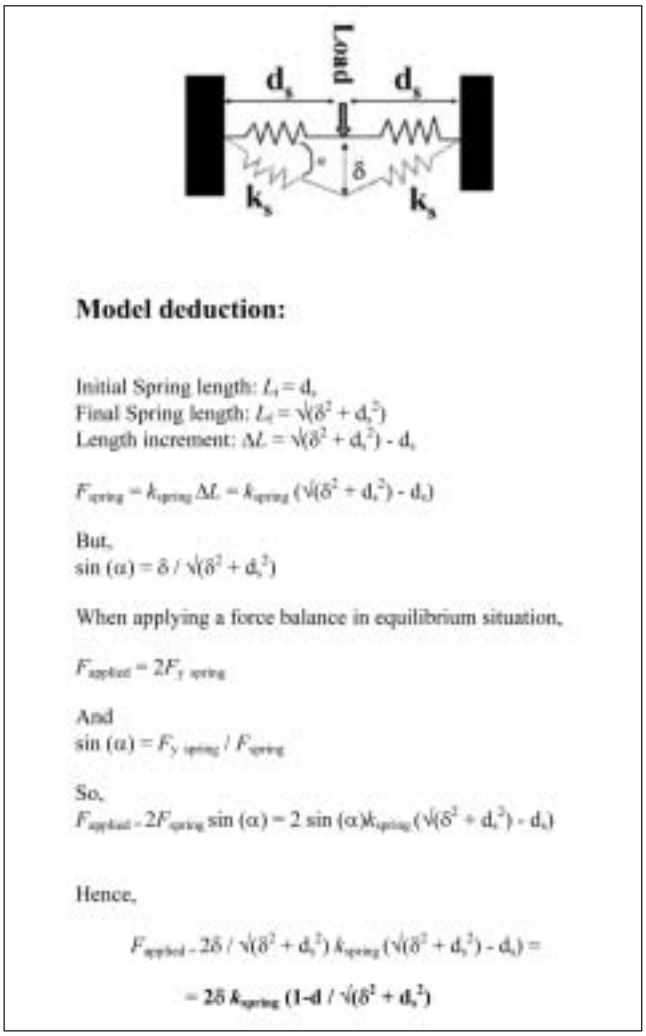

Figure 5. Mathematical deduction of the spring model proposed in the text.

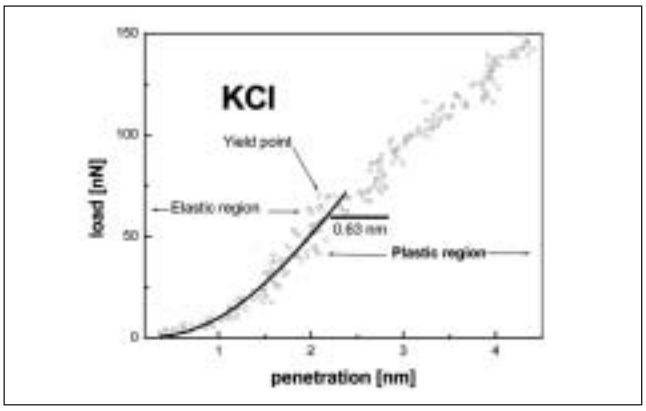

Figure 6. Nanoindentation curve for a KCl (100) single crystal surface. Solid line corresponds to least square fit to Eq. (2) in text.

outlined above: the elastic region (that has been satisfactorily fitted to our proposed model) extends up to ≈ 70 nN. At this force value the first layer break is observed, and once again it corresponds to the lattice parameter value. This is what is known as the yield point, and the plastic region extends from that force value on.

Van der Waals layered solids

Following the same philosophy as described above we investigated the mechanical response to nanoindentations of layered Van der Waals materials. This is illustrated with thin films of the molecular organic materials TTF-TCNQ and *p*-NPNN radical. Molecular organic materials are anisotropic and the films are layered with their most energetic planes (containing the shortest contacts) parallel to the substrate surface [30]. The weak interplane interactions, together with the molecular shape, produces interplanar distances in the order of 1 nm, ideal for nanoindentation experiments.

Nanoindentation and imaging were performed in normal atmospheric conditions because the material is hydrophobic. No adhesion was recorded in the force curves. Si cantilevers with a lower spring constant, around 3 Nm^{-1} (nominal values 1-5 Nm^{-1}), were used in this case. After each indentation the cantilever deflection h was calibrated using a clean glass slide, rather than a diamond thin film, in order to increase sensitivity. Imaging was performed in TM and the tip oscillation amplitude was reduced to zero while indenting.

TTF-TCNQ as a model system

TTF-TCNQ is a charge transfer salt exhibiting a monoclinic crystal structure ($P2_1/c$, a = 12.298 Å, b = 3.819 Å, c = 18.468 Å, β = 104.46º [31]) built up from parallel, segregated chains of donors (TTF) and acceptors (TCNQ). Thin films of TTF-TCNQ grown on ex situ cleaved KCl(001) substrates were obtained by thermal sublimation in high vacuum (~10^{-6} mbar). The films consist of highly oriented and strongly textured rectangular-shaped microcrystals. The molecular (002) planes (*ab*-planes) are parallel to the substrate surface and the microcrystals are oriented with their *a*- and *b*-axis parallel to both the [110] and [-110] substrate directions, respectively, due to the cubic symmetry of the substrates [32]. The substrates were held at room temperature during evaporation.

Figure 7 shows a nanoindentation curve performed on a flat, defect-free region of a thin TTF-TCNQ film. These films are stable in air, as is demonstrated by TMAFM measurements [33]. The film behaves elastically below F_y = 240 Nn (= 80 nm × 3 Nm^{-1}). In this case, the maximum elastic surface deformation, δ_y, is ~ 3.5 nm. The shape of the loading curve in the elastic region may be modeled using Hertzian theory for a paraboloid indenting a plane as discussed above. From the fit to the data we obtain E^*= 22 GPa, and taking the same values for E(tip) and ν(tip) as indicated above and estimating ν(TTF-TCNQ) by 0.4, we obtain E = 22 Gpa. This estimation is in the order of previously reported values obtained from temperature dependent measurements (E = 10 GPa) [34], from the slope of acoustic branches measured by neutron scattering on single crystals (E =20 GPa) [35], from calculations based on sound velocity using ultrasonic techniques (E = 34 GPa) [36], and on the inverse of compressibility coefficients (E = 55 GPa) [37]. The mean applied stress normal to the surface at plastic yield σ_y is 4

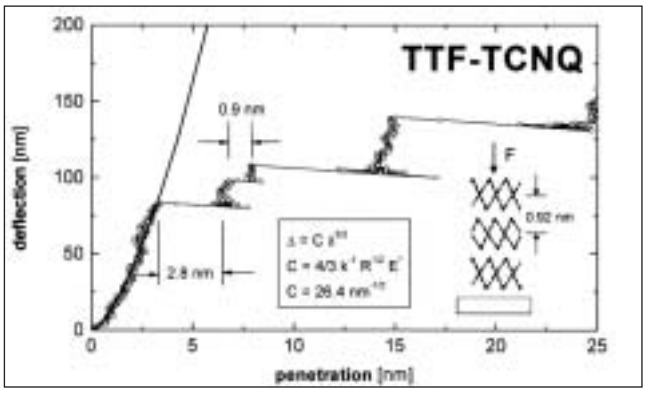

Figure 7. Nanoindentation curve (deflection vs. penetration) performed on a thin TTF-TCNQ film. The solid line represents the fit of the elastic region to the Hertzian model, which is indicated in the inset together with the value of the constant C_{fit} obtained from the fit (k ~ 3 Nm^{-1}, v ~ 7.6 μms^{-1}). Also illustrated is the direction of the applied force with regard to the molecular distribution in the film.

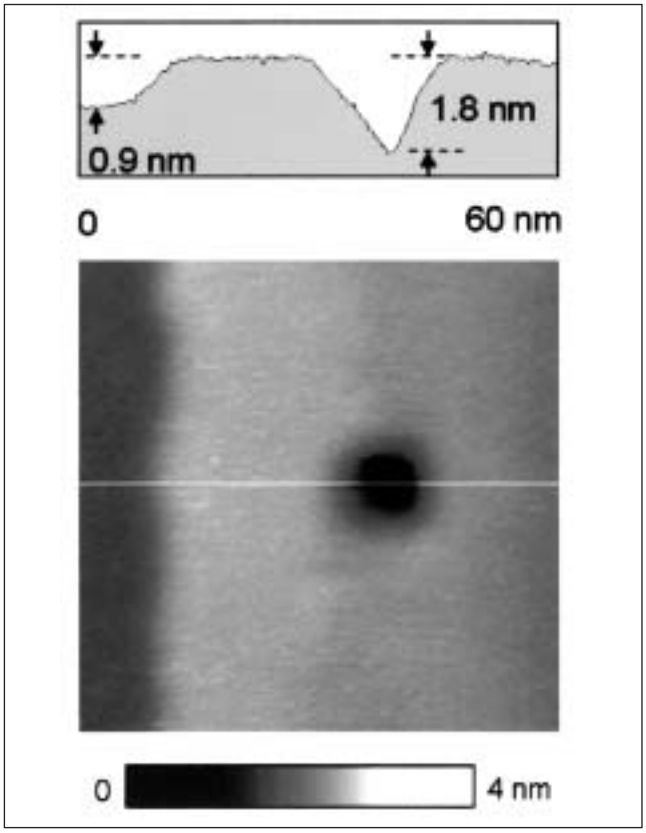

Figure 8. TMAFM image of the indented region with its corresponding line profile. The resultant plastic deformation is compared with a monomolecular step.

GPa, after averaging over several indentation curves obtained with different tips. This value is comparable to, σ_y = 7 GPa for Au(111) [38] and σ_y = 10 GPa for MgO(100). The estimated critical shear stress is τ = 2 GPa. Above σ_y, the material deforms plastically as is shown by discrete discontinuities (multiples of ≈ 0.9 nm) associated with molecular layers being expelled by the penetrating tip (the distance between two consecutive *ab*-molecular planes is 0.92 nm). This is illustrated in Fig. 7, where discontinuities of 0.9 and 2.8 nm are observed just above the yield point. In Figure 8, a TMAFM image taken after an indentation process, the plastic effect of the nanoindentation on the surface is clearly observable. The total tip penetration (~ 5 × 0.9 nm) is larger than the induced depth defect: ≈ 1.8 nm (= 2 × 0.9 nm). This, and the fact that the depth corresponds exactly to two molecular layers, suggest ordered relaxation of the material upon unloading. The close-lying step in Fig. 8 (left of image) enables heights to be accurately calibrated (step height = 0.92 nm). No indentation-induced dislocations are observed in the vicinity of the indented region and the material expelled by the penetrating tip does not form debris around the indentation. Most probably it evaporates during the subsequent scan process of image acquisition [39].

p-NPNN

Thin films of *p*-NPNN obtained by thermal evaporation in high vacuum on glass slides held at room temperature crystallize in the monoclinic α-phase. The molecular (002) planes (*ab*-planes) are parallel to the substrate surface and exhibit a high degree of orientation, but no in-plane texture [40]. Figure 9 shows a nanoindentation curve (k ~ 3 Nm^{-1}) performed on an as-grown α-phase *p*-NPNN thin film. The applied force is perpendicular to the molecular *ab*-planes. The film behaves elastically below F_y = 420 nN (= 140 nm × 3 Nm^{-1}) and the maximum elastic deformation is ca. 10 nm. A fit to the Hertzian model of the elastic response gives *E* ~ 1.7 GPa. After averaging over several indentation curves obtained with different tips we obtained σ_y ~ 1.3 GPa and τ ~ 0.6 GPa. As for TTF-TCNQ, above the yield point discrete discontinuities corresponding to multiples of the distance between two consecutive *ab*-planes (= 1.2 nm) are observed.

The nanometer scale surface morphology of the α-*p*-NPNN thin films is rather complex. It is composed of a random distribution of opposite sign dislocations (spirals)interacting in pairs (Frank-Read growth mechanism), each spiral emerging from a hollow core [41]. The relatively small distance, L, between emerging points of the interacting spirals

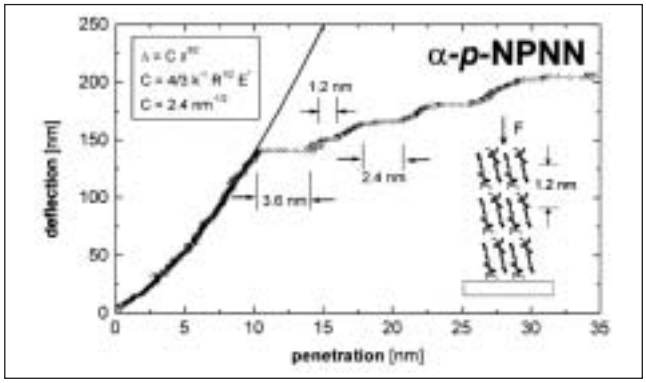

Figure 9. Nanoindentation curves (deflection vs. penetration) performed on an as-grown thin α-*p*-NPNN film. The solid line represents the fit of the elastic region to the Hertzian model, which is indicated in the inset together with the value of the constant C_{fit} obtained from the fit. (k ~ 3 Nm^{-1}, v ~ 14.0 μms^{-1}) Also illustrated is the direction of the applied force with regard to the molecular distribution in the film.

(L > 50 nm) indicates a rather high dislocation density, caused by a rapid in-plane crystallization from an initially amorphous state [42]. The α-phase transforms spontaneously into the more stable β-phase. However, this transformation is inhibited if the thickness of the as-grown α-phase films lies below a critical thickness (~ 1 μm). The stabilization, which is induced by residual stress after growth [43], allows physical properties of this otherwise metastable phase to be determined. The accumulated stress field after growth induces an increase in activation energy of critical nuclei formation from the β-phase to the α-phase matrix, and thus enables inhibition of this solid-solid phase transition.

No experimental determinations of E, σ_y and τ are available for single crystals of α-*p*-NPNN due to their rapid transformation to the β-phase. The residual stress after growth may contribute to the estimated values of such parameters for thin films, since defects hinder the propagation of dislocations. This could be modeled by the Hall-Petch equation, $\sigma_y \approx \sigma_y^{int} + K L^{-1/2}$, valid for grain boundaries, where σ_y^{int} and K represent the intrinsic stress (low dislocation density) normal to the surface at plastic yield and a constant, respectively, and where the grain size is replaced by the distance between dislocations [44]. Thermal stress is negligible because the substrates are held at room temperature during growth.

Concluding comments

Indentation description of materials has become an easy way of determining the mechanical properties of solids, but different models need to be applied to the results in order to explain cavity formation during indentation. The observed phenomena include the formation of dislocations and the energy transferred to the solid in order for the material to flow around the indenter, forming debris. Nanoindenters have been used to describe different regions in a monocrystal surface, such as the different response to indentation on a Au(111) terrace, either far from or close to a step[10]. A nanoindentation of a few nanometers on Au(111) generates new steps along certain preferred directions [45] due to the ductile character of metals, which enables them to rearrange easily before flowing under the pressure exerted by the tip. Brittle materials do not have this ability and, as demonstrated by our results, no dislocations or step generation are observed. We have shown that the loading curve in the indentation plot is not a continuous change, as described in microindentation experiments [4], but rather a series of discontinuities corresponding to successive breaks of material layers interspersed with elastic deformation of the uppermost layer. Thus, the first break observed after the elastic regime of the surface can be considered as the critical stress of plastic deformation. Given how the loading curve operates, we concluded that the breaks are always produced at the same critical stress.

The difficulty of synthesizing sufficiently large single crystals of molecular organic materials hinders the description of several physical properties, and parameters associated with mechanical properties cannot be obtained by conventional methods. As demonstrated, however, such parameters can be estimated by means of nanoindentation performed on thin films, which provide larger areas of highly oriented and crystalline domains of the precursor materials. Thin film growth also offers the possibility of stabilizing metastable phases. Determining the physical properties of such phases cannot be done with single crystals because of their intrinsic instability. In the case of TTF-TCNQ, our experimentally obtained values lie within the range of currently published data for large single crystals. To our knowledge, no such information from single crystals is available for α-*p*-NPNN.

Acknowledgements

This work was mainly financed by the Generalitat de Catalunya. The authors thank the SCT of the University of Barcelona for providing equipment.

References

[1] D. Tabor, *Gases, liquids and solids and other states of matter, 3rd ed*, Cambridge University Press, Cambridge, 1991, Chaps. 7 &8

[2] J. Pethica, R. Hutchings and W.C.Oliver, Philos. Mag. A48, 593(1983)

[3] D. Newey, M.A. Wilkins and H.M. Pollock, J. Phys. E 15, 119 (1982)

[4] T.F. Page, W.C. Oliver and C.J. McHargue, J. Mat. Res. 7, 450 (1992)

[5] Q. Ma and D.R. Clarke, J. Mat. Res., 10, 853 (1995)

[6] R. C. Thomas, J. E. Houston, T. A. Michalske, and R. M. Crooks, Science 259, 1883 (1993).

[7] J. D. Kiely, R. Q. Hwang, and J. E. Houston, Phys. Rev. Lett. 81, 4424 (1998).

[8] S. G. Corcoran, R. G. Colton, E. T. Lilleodden, and W. W. Gerberich, Phys. Rev. B 55, 16057 (1997).

[9] P. Tangyunyong, R. C. Thomas, J. E. Houston, T. A. Michalske, R. M. Crooks, and A. J. Howard, Phys. Rev. Lett. 71, 3319 (1993).

[10] J. D. Kiely and J. E. Houston, Phys. Rev. B 57, 12588 (1998).

[11] Q. Dai, J. Hu, and M. Salmeron, J. Phys. Chem. B 101,1994(1997).

[12] a) H. Shindo, M. Ohashi, K. Baba, and A. Seo, Surf. Sci. 358,111(1996).b) H. Shindo, M. Ohashi, O. Tateishi, and A. Seo, J. Chem. Soc. Faraday Trans. 93(6), 1169(1997)

[13] S.L. King, M.R. Wilby and I.W. Boyd, J. Mat. Sci. & Eng. B37, 162 (1996)

[14] K. Sangwal, F. Sanz, J. Servat and P. Gorostiza, Surf. Sci. 383, 78 (1997) b) K. Sangwal, P. Gorostiza and F. Sanz, Surf. Sci. 442, 161(1999) c)N. Ikemiya, A. Kitamura and S. Hara, J. Cryst. Growth 160, 104 (1996)

[15] E. Perrot, M. Dayez, A. Humbert, O. Marti, C. Chapon, and C. R. Henry, Europhys. Lett. 26, 659 (1994).

[16] J. Fraxedas, S. Garcia-Manyes, P. Gorostiza and F. Sanz, Proc. Natl. Acad. Sci USA 99, 5228 (2002).
[17] P.F.M. Teran Arce, G. Andreu, P. Gorostiza and F. Sanz, Appl.Phys. Lett. 77, 839 (2000).
[18] S. Timoshenko and J. N. Goodier, *Theory of Elasticity*, 2nd edition (McGraw-Hill, New York, 1951), Vol. 1, p.372.
[19] N. A. Burnham, R.J. Colton and H. M. Pollock, Nanotechnology 4, 64 (1993).N. A. Burnham, O. P. Behrend, F. Oulevey, G. Gremaud, P. J. Gallo, D. Gourdon, E. Dupas, A. J. Kulik, H. M. Pollock, and G. A. D. Briggs, Nanotechnology 8, 67 (1997).
[20] J. H. Hoh and A. Engel, Langmuir 9,3310 (1993).
[21] S. M. Hues and C. F. Draper, in *Procedures in SPMs,* Wiley, Chichester, U.K., (1998), Chap. 9.
[22] *Handbook of Chemistry and Physic*s, 79th ed., edited by D. R. Lide (CRC, Boca Raton, FL, 1999).
[23] A. Folch, P. Gorostiza, J. Servat, J. Tejada, and F. Sanz, Surf. Sci. 380, 427 (1997).
24] However, during indentation experiments performed on Au(111) terraces, prior to cavity formation we observed the formation of steps along specific crystallographic directions. (Unpublished results).
[25] Hertz, H., *Miscellaneous papers*, Macmillan & Co., London, 1896.
[26] Chang-Sheng Zha, Ho-kwang Mao, and Russell J. Hemley, Proc. Nat. Acad. Sciences 97, 13494 (2000).
[27] *Landolt-Börnstein, Numerical Data and Functional Relationships in Science and Technology, Group III: Crystal and Solid State Physics*, 1st edition, edited by O. Madelung (Springer-Verlag, Berlin, 1982), Vol. 17.
[28] K. J. Johnson, *Contact Mechanics*, Cambridge University Press, UK, (1995).
[29] J. Caro, J. Fraxedas, P. Gorostiza, and F. Sanz, J. Vac. Sci. Technol. A 19, 1825 (2001).
[30] S. Molas, J. Caro, J. Santiso, A. Figueras, J. Fraxedas, M. Fourmigué, C. Mézière and P. Batail, J. Cryst. Growth 218, 399 (2000).
[31] T. J. Kistenmacher, T. E. Philips, and D. O. Cowan, Acta Crystallogr. B 30, 763 (1974).
[32] J. Fraxedas, J. Caro, A. Figueras, P. Gorostiza, and F. Sanz, J. Vac. Sci. Technol. A16, 2517 (1998).
[33] J. Fraxedas, J. Caro, A. Figueras, P. Gorostiza, and F. Sanz, Surf. Sci. 395, 205 (1998).
[34] J. C. Phillips, J. Solid State Chem. 20, 211 (1977).
[35] J. P. Pouget, S. M. Shapiro, G. Shirane, A. F. Garito, and A. J. Heeger, Phys. Rev. B 19, 1792 (1979).
[36] T. Tiedje, R. R. Haering, M. N. Jericho, W. A. Roger, and A. Simpson, Solid State Commun. 23, 713 (1977).
[37] A. Filhol, G. Bravic, J. Gaultier, D. Chasseau, and C. Vettier, Acta Cryst. B 37, 1225 (1981).
[38] J. D. Kiely and J. E. Houston, Phys. Rev. B 57, 12588 (1998).
[39] H. P. Lang, B. Erler, A. Rossberg, M. Piechotka, E. Kaldis, and H. J. Güntherodt, J. Vac. Sci. Technol. B 14, 970 (1996).
[40] J. Caro, J. Fraxedas, O. Jürgens, J. Santiso, C. Rovira, J. Veciana, and A. Figueras, Adv. Mater. 10, 608 (1998).
[41] J. Fraxedas, J. Caro, A. Figueras, P. Gorostiza, and F. Sanz, Surf. Sci. 415, 241 (1998).
[42] J. Caro, J. Fraxedas, and A. Figueras, J. Cryst. Growth 209, 146 (2000).
[43] J. Fraxedas, J. Caro, J. Santiso, A. Figueras, P. Gorostiza, and F. Sanz, Europhys. Lett. 48, 461 (1999).
[44] M. Ohring, *The Materials Science of Thin Films*, 1st edition (Academic Press, San Diego, 1992), Vol. 1, Chap. 9, p.409.
[45] P.F.M. Teran Arce, P. Gorostiza and F. Sanz, unpublished results.

About the authors

Sergi Garcia-Mañes (Barcelona, 1978) graduated in chemistry from the Universitat de Barcelona in 2000, having specialised in analytical and physical chemistry. He received the First in Graduating Class Award. He is now a PhD student with a grant obtained from the Generalitat de Catalunya. His doctoral work is based on atomic force spectroscopy (SPM) and his main interest is in nanomechanics and single molecule manipulation. This work is being carried out part-time in the Universitat de Barcelona and the University of California at Berkeley.

Pau Gorostiza (Barcelona, 1969) graduated in physics from the University of Barcelona (UB) in 1992. His postgraduate work was carried out in the departments of Physical Chemistry and Electronics, where he focused on electrochemistry and the physics of semiconductor-liquid interfaces. He received his PhD from the University of Barcelona in 1999. Since 1996 he has also worked in the SPM Laboratory at the Serveis Cientificotècnics, UB. His current research interests include bioelectronic interphases for applications in nanotechnology. In 2000, he received the Young Biomedical Researcher Award from the Francisco Cobos Foundation. He currently holds a postdoctoral post at the University of California at Berkeley.

Jordi Fraxedas (Tarragona, 1962) graduated in physics from the University of Zaragoza in 1985 and obtained his PhD (Dr. rer. nat.) in 1990 from the University of Stuttgart (Germany). His thesis work (photoemission on semiconductor surfaces) was performed at the Max Planck Institut für Festkörperforschung and at the Berliner Speicherring für Synchrotronstrahlung (BESSY), under the supervision of Prof. Dr. M. Cardona. After holding a post-doctoral post at the European Synchrotron Radiation Facility (ESRF) (1991-1992) and being an Established Researcher at the European Laboratory for Particle Physics (CERN) (1993-1994), he is now a tenured scientist at the Institut de Ciència de Materials de Barcelona (ICMAB), part of the Consejo Superior de Investigaciones Científicas (CSIC). His main research field is surface science, and in the last few years he has been working on thin molecular organic films.

Fausto Sanz (Barcelona, 1948) graduated in chemistry in 1971 from the University of Barcelona (UB), and obtained his PhD in 1975 from the same university. He is Full Professor and currently teaches in the Department of Physical Chemistry, UB, in the fields of surface science, electrochemistry and SPM applications. Visiting Investigator at the University of Utrecht (The Netherlands)(1985-1986) and Visiting Scholar at the Lawrence Berkeley Laboratory (University of California at Berkeley)(1991-1992), his research started in electrochemistry and progressively developed to include surface science using nanoprobes. He is currently involved in a biointerphases project, having joined the «Research Center for Bioelectronics and Nanobioscience», recently created by the UB in order to provide an interdisciplinary focus on experimental molecular and cell control and manipulation. He is an active member of the Northern California Chapter of the AVS and of the Electrochemical Society.